Controlling Macroscopic Friction through Interfacial Siloxane Bonding

Liang Peng,[1,*] Chao-Chun Hsu,[2] Chen Xiao,[3,1] Daniel Bonn,[1] and Bart Weber[3,1]

[1]*Van der Waals-Zeeman Institute, Institute of Physics, University of Amsterdam, Science Park 904, 1098 XH Amsterdam, The Netherlands*

[2]*Van't Hoff Institute for Molecular Sciences, University of Amsterdam, 1098 XH Amsterdam, The Netherlands*

[3]*Advanced Research Center for Nanolithography (ARCNL), Science Park 106, 1098 XG Amsterdam, The Netherlands*

(Received 24 April 2023; accepted 12 October 2023; published 29 November 2023)

Controlling macroscopic friction is crucial for numerous natural and industrial applications, ranging from forecasting earthquakes to miniaturizing semiconductor devices, but predicting and manipulating friction phenomena remains a challenge due to the unknown relationship between nanoscale and macroscopic friction. Here, we show experimentally that dry friction at multiasperity Si-on-Si interfaces is dominated by the formation of interfacial siloxane (Si─O─Si) bonds, the density of which can be precisely regulated by exposing plasma-cleaned silicon surfaces to dry nitrogen. Our results show how the bond density can be used to quantitatively understand and control the macroscopic friction. Our findings establish a unique connection between the molecular scale at which adhesion occurs, and the friction coefficient that is the key macroscopic parameter for industrial and natural tribology challenges.

DOI: 10.1103/PhysRevLett.131.226201

Friction at multiasperity interfaces is a fundamental problem in tribology that has practical importance in a wide range of industries, consuming more than 20% of global energy [1]. Despite the significant efforts devoted to understanding friction since the time of Leonardo da Vinci, the quantitative prediction of macroscopic friction forces from first principles remains a challenging task [2–8]. Recent advances in nanoscale friction experiments and molecular dynamics simulations have shed light on the fundamental mechanisms of friction at single asperity contacts, revealing that Van der Waals interactions [9], together with interfacial bond networks [10–13] such as covalent [14–19] and hydrogen [20–22] bonds can play a dominant role in determining adhesion and friction. However, the relation between the number of interfacial bonds and the measured friction force at the microscopic scale is still unknown. Moreover, it is unclear whether the bonding mechanisms responsible for nanoscale friction control friction at larger, application-relevant scales [23].

Understanding the relationship between chemical bonding and macroscopic friction is a significant challenge faced by scientists across various disciplines, including physics, chemistry, and geology. Several factors can influence friction, including wear particles, contamination, contact plasticity, and adhesion [2,24]. Moreover, the roughness of extended interfaces creates a multitude of contact points that are often obscured by the bulk contacting bodies, making it difficult to directly observe contact phenomena [25–27]. These challenges are particularly significant when studying silicon-based materials, given their widespread use in the semiconductor industry and their involvement in the generation of earthquakes [28]. Additionally, the surface chemistry of oxidized silicon is notoriously difficult to control and quantify, involving dehydroxylation-hydroxylation reactions between various functional silanol groups and siloxane bridges that are dependent on environmental factors [29–31]. Thus, establishing a direct relationship between interfacial bonding and macroscopic friction remains a daunting task.

In this Letter, we experimentally show that macroscopic Si-on-Si friction emerges from the formation and rupture of interfacial siloxane bonds and can thus be controlled through surface chemistry. Si-on-Si friction was measured using a rheometer (DSR 502, Anton Paar) inside a customized environmentally controlled chamber, as shown in Fig. 1(a). The rheometer can be used to rotate at precisely controlled speeds while simultaneously measuring the shear and normal forces, allowing one to infer the friction coefficient. Before entering the environmental chamber for the friction experiments, the silicon balls (Goodfellow) were sonicated in ethanol and then Milli-Q water, followed by nitrogen flow drying. In the friction experiments, a cleaned silicon ball (with a native oxide layer) was brought into contact with an as-received p-doped silicon (100) wafer (from University Wafer) covered with a native oxide layer. Before the contact was formed, the surfaces were equilibrated under the dry nitrogen environment inside the humidity-controlled chamber for 1 h. The contact was then formed under a normal load of 40 mN. According to contact calculations, discussed later in the text, the average asperity scale contact pressure was 3.6 GPa, similar to the pressures exerted at single-asperity contacts in AFM measurements [11,32]. The sliding speed of the silicon ball on the silicon wafer imposed by the rheometer was

 © 2023 American Physical Society

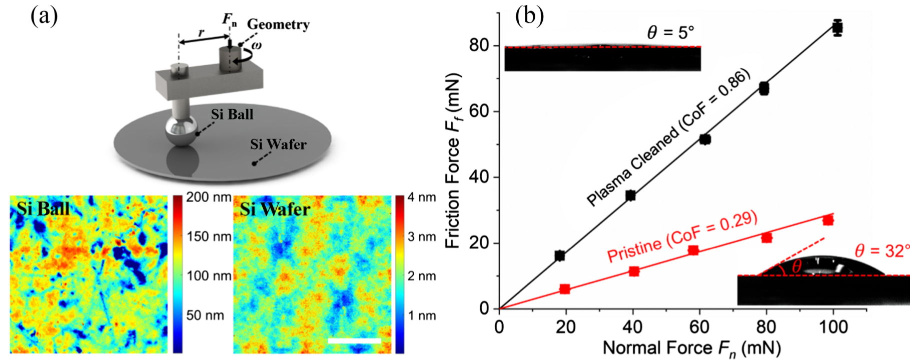

FIG. 1. Experimental system (a) and enhanced friction upon plasma cleaning of silicon surfaces (b). (a) Top: a 3-mm-diameter silicon ball inside a humidity-controlled chamber is clamped to the geometry of a rheometer and brought into contact with a silicon wafer. The distance (r) between the rotation axis and the silicon ball is 10 mm. By lowering and rotating the rheometer tool at a constant angular velocity (ω), the normal force (F_n) and friction force (F_f) on the contact can be measured simultaneously at an imposed sliding speed (ωr) . Bottom: AFM images of the silicon ball (bottom left) and silicon wafer (bottom right). The rms roughness of the surfaces is 40.5 nm (ball) and 0.5 nm (wafer), measured over an area of 31.13×31.13 μm^2, corresponding to the average roughness (Ra) of 26 and 0.6 nm, respectively. The small changes in surface roughness induced by the plasma treatment are reported in Fig. S3. Scale bar, 10 μm. (b) Friction force (F_f) as a function of normal load (F_n), measured in the dry nitrogen environment (RH = 0.8%). The ratio of these two forces gives the coefficient of friction (CoF), $\mu = F_f/F_n$. The red and black data correspond to the friction force measured with pristine and with oxygen plasma-cleaned silicon surfaces, respectively. Insets display water contact angle (θ) images on wafer surfaces in the dry nitrogen environment (RH = 0.8%) before (bottom) and after (top) plasma cleaning, in which the average measured θ are 32° and 5°, respectively. All the reported water contact angles represent the average of three measurements.

varied from 0.1 to 10 μm/s in the velocity-dependent experiments and kept constant at 0.1 μm/s in all other experiments. The reported steady-state friction forces were averaged over four sliding strokes (Fig. S1 [33]). All strokes were kept as short as 2 μm, and measured on previously untouched areas of the silicon wafer. This "nonrepeated" measurement protocol is applied to minimize the influence of wear, which induces smoothening at the nanoscale [34], on the experiments (Fig. S2). During drying and equilibration, in between the measurements, the silicon ball was separated from the wafer. To investigate the influence of surface chemistry on friction, we repeated the friction experiments with oxygen plasma-cleaned silicon balls and wafers; plasma cleaning is commonly used to chemically modify hydrophilic surfaces [41–43]. The oxygen plasma activation was conducted inside a reactor (Zepto One, Diener Electronic) at a vacuum pressure of 0.1 bar and frequency of 50 Hz for 5 m.

As shown in Fig. 1(b), the plasma surface treatment results in an almost 300% increase in dry Si-on-Si friction under various applied normal loads. While the friction increases significantly upon plasma cleaning, the average water contact angle, measured using an optical contact angle goniometer (Easy Drop, Kruss), decreases markedly upon plasma treatment.

The plasma-cleaning-induced hydrophilicity is known to decrease over time when the plasma-cleaned surfaces are exposed to the environment [44,45]. We, therefore, track the evolution of the friction force as a function of the time during which the plasma-cleaned silicon surfaces are exposed to dry nitrogen. As shown in Fig. 2, the friction force gradually decreases with nitrogen drying time while the water contact angle increases. In contrast, the water contact angle and the friction force remained constant over a period of 6 h in a control experiment conducted at a relative humidity of 40% (Fig. S4). Given the thermodynamic stability of hydroxylated surfaces [46,47], we interpret these results as follows. In the dry environment, the increase in water contact angle is likely driven by the

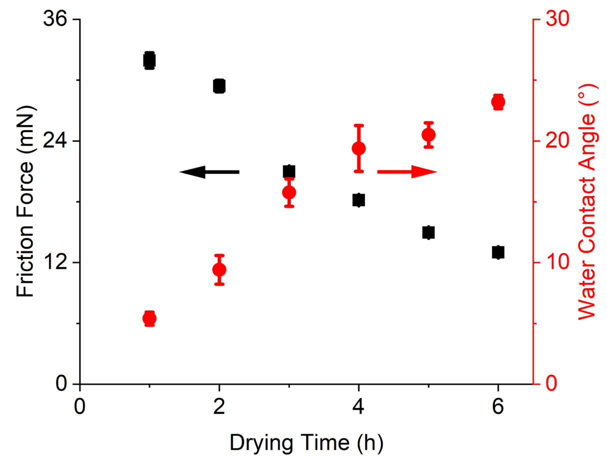

FIG. 2. Friction force as a function of the time during which the surfaces were in contact with dry nitrogen (<0.8% relative humidity). Friction measurements were performed on the plasma-cleaned silicon surfaces at a normal load of 40 mN after different nitrogen drying times (see also Fig. S1). The water contact angles corresponding to the nitrogen drying times are indicated by the red data points.

displacement of the hydroxyl groups by carbonaceous contamination due to air exposure [48]. However, this process is blocked or delayed in a humid environment as the absorbed water layers on a wafer could potentially shield the hydroxylated surface from contamination [31], resulting in a stable water contact angle during the aging process.

The clear correlation between surface chemistry, as quantified by the water contact angle, and friction force in Fig. 2 suggests that the dry friction is dominated by the interfacial chemical state. Therefore, we hypothesize that the formation of interfacial Si─O─Si bonds from OH groups (thereby releasing a water molecule) on the two opposite surfaces controls the macroscopic friction force, in analogy to previously proposed nanofriction mechanisms [15,17,49]. To test this hypothesis, a quantitative connection between the observed water contact angle and the density of surface OH groups on the surfaces is necessary. To determine the surface OH density, we can use the water contact angle measurements if the chemically heterogeneous silicon surface is composed of a fraction f of silanol (Si─OH) groups and a fraction, $(1-f)$, of siloxane (Si─O─Si) groups. We can then use a Cassie-Baxter model [50] to express the equilibrium water contact angle (θ) on the silicon surfaces as

$$(1+\cos\theta)^2 = f\times(1+\cos\theta_1)^2 + (1-f)\times(1+\cos\theta_2)^2, \tag{1}$$

where θ_1 and θ_2 are the water contact angles on the pure homogeneous surfaces fully covered with Si─OH groups or Si─O─Si groups, respectively. Plasma activation [51] and thermal treatment [52] are two reported methods to reach these two extreme surface chemistry states, respectively. The surface OH density on the surface is set to be 0 $\mathrm{OH\,nm^{-2}}$ after thermal treatment and 4 $\mathrm{OH\,nm^{-2}}$ after plasma cleaning, respectively [53].

As shown in Fig. 3, the Cassie-Baxter model describes the data well, and shows how the water contact angle increases nonlinearly as the density of OH groups decreases. To experimentally test the accuracy of this prediction, we quantify the surface OH density through fluorescence labeling experiments [54], in which fluorescent molecules (Rhodamine 101) are covalently bonded to surface OH groups through APTES molecules. To quantify the change of surface OH density on the plasma-cleaned wafer with nitrogen drying time, fluorescence detection was carried out using a confocal microscope (MicroTime200, PicoQuant GbmH) with an extended spectrometer. To avoid any damage to the surface, the fluorescence labeling of the surface OH groups was carried out in two steps. Before the fluorescence measurement, seven plasma-cleaned wafers were held inside a drying chamber for different times, corresponding to different nitrogen drying times in the friction experiments, followed by *in situ* chemical vapor

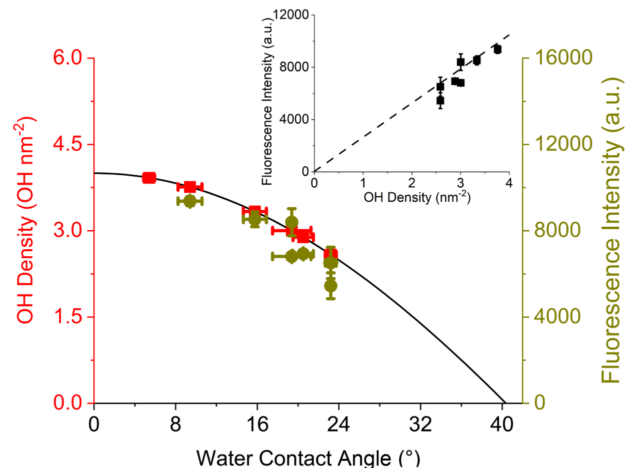

FIG. 3. Modeling and measurement of the surface OH density. The surface OH density (red data) is calculated using the Cassie-Baxter model (black solid line) and the measured water contact angles. The OH density was also measured through fluorescence labeling (dark yellow circles). The upper right inset shows the linear relationship between the measured fluorescence intensity and the modeled OH density.

deposition (CVD) with APTES [55]. The amine groups on the deposited monolayer APTES [55] were then functionalized with Rhodamine 101 through liquid immersion [56]. Subsequently, the fluorescence spectra on the wafers were measured with a fixed power excitation at 545 nm after any Rhodamine 110 residues were removed. The surface density of OH groups can thus be quantified by measuring the fluorescence intensities of the bonded rhodamine molecules (Fig. S5). The experimentally measured fluorescence intensity is found to agree well with the surface OH density predicted by the Cassie-Baxter model (Fig. 3, inset), confirming the relation between wettability and surface density of OH molecules.

The observed strong increase in friction when increasing surface OH density then suggests that in our system the friction is due to Si─O─Si bonds formed across the interface, thus increasing the adhesion between the two contacting surfaces. This poses the question of how to quantify adhesion. For multicontact interfaces, the adhesion measured upon unloading is influenced by the elastic energy stored in asperity deformations, the so-called "adhesion paradox" [57,58]; this greatly complicates the direct measurement of interfacial bond strength through pull-off experiments [59]. In our case, we can then test if the macroscopic friction force is indeed generated by forming and rupturing the interfacial Si─O─Si bonds by plotting the interfacial shear stress against the density of interfacial Si─O─Si bonds in Fig. 4. The frictional shear stress is defined as the measured macroscopic friction force divided by the calculated area of real contact. The latter is estimated using a boundary element method (BEM, Tribology Simulator [33]) [22,60], in which the measured

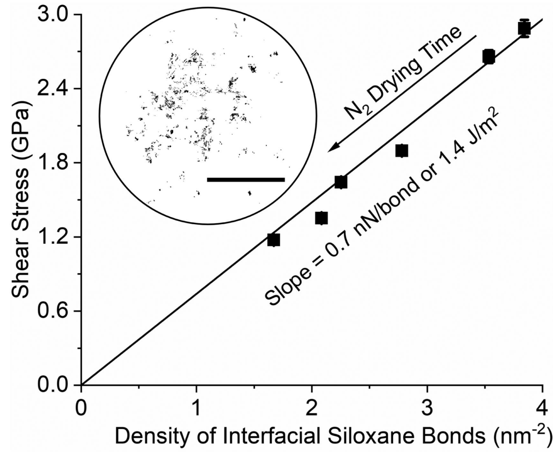

FIG. 4. Frictional shear stress as a function of the interfacial siloxane density. The slope of the solid line represents the bond rupture force of a single interfacial Si—O—Si bond. The black area in the upper circular inset displays the area of real contact calculated using the boundary element method at a load of 40 mN. Scale bar, 10 μm.

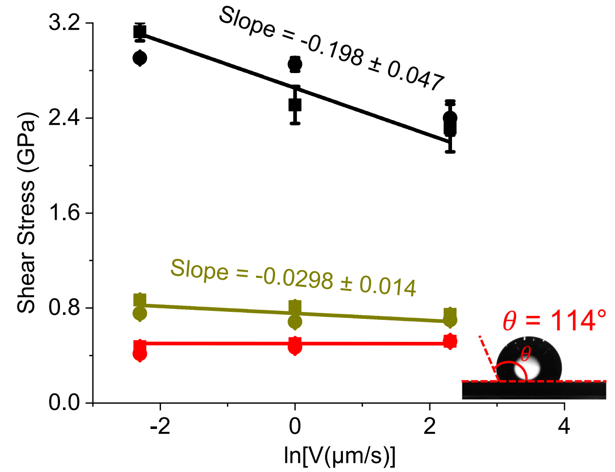

FIG. 5. Dependence of the frictional shear stress on sliding velocity. The friction force was measured at increasing (squares) and decreasing (solid circles) velocities ranging from 0.1 to 10 μm/s at a load of 40 mN. The frictional shear stress is defined as the measured friction force divided by the calculated area of real contact. The surfaces were plasma-cleaned silicon surfaces after drying for 1 h at a relative humidity of 0.8% (black data symbols), after drying for 6 h (dark yellow), and with a monolayer of hydrophobic CVD coating (red, see main text for details), respectively. The nonbonding frictional shear stress (0.4 GPa) observed at the hydrophobically coated interfaces is small compared to the bonding-induced shear stress (3 GPa) and therefore only has a minor impact on our bonding analysis. The inset displays the water contact angle (θ) image on the hydrophobically coated wafer, in which the measured θ is around 114°.

surface topography and the mechanical properties of silicon (Young's modulus $E = 130$ GPa, Poisson's ratio $\nu = 0.2$, Hardness $H = 10$ GPa) are used as input to describe the roughness scale elastic deformations at the interface (see details in Supplemental Material, Sec. 1). The interfacial Si—O—Si bond density is assumed to be proportional to the probability that two OH groups on the opposite surfaces meet at the interface. Therefore, the interfacial Si—O—Si bond density should scale with the square of the OH density on a single surface, with a maximum of 4 Si—O—Si bonds per nm^2 when both surfaces are fully covered by Si—OH groups [53]. We observe a convincing linear relation between the shear stress and the interfacial Si—O—Si density with a proportionality constant of 0.7 nN/bond or 1.4 J/m^2 (Fig. 4), which is comparable to the previously reported strength of a single interfacial Si—O—Si bond of 1.4 nN/bond [59] and Si—O—Si bonding energy of 1.5 J/m^2 [61]. As the bond rupture process is different in our experiment compared to the atomic force microscopy characterization of bond strengths reported in Ref. [59], the discrepancy between the values is not surprising. We thus conclude that the macroscopic friction force is indeed dominated by the formation and rupture of interfacial Si—O—Si bonds.

To test this conclusion further, we performed velocity-dependent friction experiments in which each stroke was measured on a previously untouched spot on the wafer. As shown in Fig. 5, the measured friction at the plasma-cleaned interfaces decreases with increasing sliding velocity in the range of 0.1 to 10 μm/s. Furthermore, this velocity-weakening effect diminishes as the density of surface OH groups is decreased by exposing the plasma-cleaned surfaces to a dry environment. The observed small hysteresis during increasing-decreasing velocity may be attributed to changes in drying time-dependent surface chemical state, as the hysteresis decreases when the surface chemical state gradually stabilized after 6 h nitrogen drying. Finally, when the silicon surfaces are functionalized with a monolayer of hydrophobic CVD coatings (1H, 1H, 2H, 2H-perfluorooctyltrichlorosilan), the velocity dependence of the friction completely disappears. These observations are consistent with the predictions of the phenomenological rate and state friction model, which postulates that dynamic friction scales with the logarithm of the sliding velocity [62,63]. For the velocity-weakening friction, it is commonly interpreted that the dynamic friction force is limited by the rate at which interfacial bonds can be formed: lower sliding speeds enable more interfacial bonds to be formed and thus lead to higher friction [15,32,49]. Assuming the reaction kinetics of an interfacial siloxane bond follows the Arrhenius behaviors as proposed previously in a multibond model [12,64], we can quantitatively estimate the number of interfacial bonds per unit contact area $[P(t)]$ by using the logarithm of contact time (t),

$$P(t) \propto \frac{N_0}{G} k_B T \ln(t), \tag{2}$$

Where N_0 is the total number of available bonding sites per nm^2 with an energy barrier of G at the beginning of sliding, k_B is Boltzmann's constant, and T is the temperature, 293 K. Substituting the contact time t with the typical lifetime, (D/V), of an interfacial Si─O─Si bond with size D during sliding at velocity V, the interfacial shear stress (τ) can thus be obtained:

$$\tau \propto \frac{N_0}{G} k_B T f_0 \ln\left(\frac{D}{V}\right). \tag{3}$$

Equation (3) predicts that the slope in the shear stress vs $\ln(V)$ curve should be $-(N_0/G)k_B T f_0$, where $f_0 \approx 0.7$ nN is the single interfacial Si─O─Si bond strength. Applying Eq. (3) to the experimental velocity-dependent friction data obtained after plasma cleaning and drying for 1 h (black data in Fig. 5), we extract an energy barrier for bond formation of 0.35 eV, of the same order as the previously reported energy barrier (0.5 to 1.4 eV) for the formation of interfacial Si─O─Si bonds in nanofriction experiments [32,65].

In conclusion, we find that the variation of dry friction at plasma-activated multiasperity Si-on-Si interfaces is controlled by the density of surface OH groups that can engage in the formation of interfacial Si─O─Si bonds. As the silicon surfaces are exposed to dry nitrogen, the surface OH group density and thus friction decrease. By quantifying the density of surface OH groups experimentally, we showed that the interfacial shear stress, and thus macroscopic friction force, scales linearly with the density of interfacial Si─O─Si bonds. Notably, these interfacial bonds could also be formed and broken in rolling friction. However, in order to roll over a distance of approximately an atomic spacing, only those bonds located at the trailing edge of the contact would have to be broken. Consequently, rolling would require much less external frictional force per unit displacement compared to sliding friction. Our study directly connects a fundamental understanding of nanofriction to the macroscopic friction forces that influence precision positioning, for instance in the semiconductor industry, thereby opening up new avenues for predicting and controlling friction.

We thank Albert M. Brouwer, Joshua Dijksman, and Emilia Olsson for valuable discussions and suggestions. L. P. acknowledges funding from the China Scholarship Council. C.-C. H. acknowledges funding from the Dutch Research Council (NWO) in the framework of the ENW PPP Fund for the top sectors and from the Ministry of Economic Affairs in the framework of the "PPS-Toeslagregeling."

[*]Corresponding author: l.peng@uva.nl

[1] K. Holmberg and A. Erdemir, Influence of tribology on global energy consumption, costs and emissions, Friction **5**, 263 (2017).

[2] C. M. Mate and R. W. Carpick, Tribology on the Small Scale—A Modern Textbook on Friction, *Lubrication, and Wear* (Oxford University Press, Oxford, 2019), 10.1093/oso/9780199609802.001.0001.

[3] B. Lorenz, B. N. J. Persson, G. Fortunato, M. Giustiniano, and F. Baldoni, Rubber friction for tire tread compound on road surfaces, J. Phys. Condens. Matter **25**, 095007 (2013).

[4] M. Scaraggi and B. N. J. Persson, Friction and universal contact area law for randomly rough viscoelastic contacts, J. Phys. Condens. Matter **27**, 105102 (2015).

[5] S. M. Rubinstein, G. Cohen, and J. Fineberg, Detachment fronts and the onset of dynamic friction, Nature (London) **430**, 1005 (2004).

[6] M. H. Müser, L. Wenning, and M. O. Robbins, Simple microscopic theory of Amonton's laws for static friction, Phys. Rev. Lett. **86**, 1295 (2001).

[7] E. Soylemez and M. P. De Boer, Modeling capillary bridge dynamics and crack healing between surfaces of nanoscale roughness, J. Micromech. Microeng. **27**, 125023 (2017).

[8] E. Gnecco, R. Bennewitz, T. Gyalog, and E. Meyer, Friction experiments on the nanometre scale, J. Phys. Condens. Matter **13**, R619 (2001).

[9] M. Lessel, P. Loskill, F. Hausen, N. N. Gosvami, R. Bennewitz, and K. Jacobs, Impact of Van der Waals interactions on single asperity friction, Phys. Rev. Lett. **111**, 035502 (2013).

[10] W. Zhong and D. Tomanek. First principles theory of atomic-scale friction, Phys. Rev. Lett. **66**, 965 (1991).

[11] Q. Li, T. E. Tullis, D. Goldsby, and R. W. Carpick, Frictional ageing from interfacial bonding and the origins of rate and state friction, Nature (London) **480**, 233 (2011).

[12] A. E. Filippov, J. Klafter, and M. Urbakh, Friction through dynamical formation and rupture of molecular bonds, Phys. Rev. Lett. **92**, 135503 (2004).

[13] A. L. Barnette, D. B. Asay, D. Kim, B. D. Guyer, H. Lim, M. J. Janik, and S. H. Kim, Experimental and density functional theory study of the tribochemical wear behavior of SiO_2 in humid and alcohol vapor environments, Langmuir **25**, 13052 (2009).

[14] A. Li, Y. Liu, and I. Szlufarska, Effects of interfacial bonding on friction and wear at silica/silica interfaces, Tribol. Lett. **56**, 481 (2014).

[15] Y. Liu and I. Szlufarska, Chemical origins of frictional aging, Phys. Rev. Lett. **109**, 186102 (2012).

[16] Z. Li and I. Szlufarska, Chemical creep and its effect on contact aging, ACS Mater. Lett. **4**, 1368 (2022).

[17] L. Chen, J. Wen, P. Zhang, B. Yu, C. Chen, T. Ma, X. Lu, S. H. Kim, and L. Qian, Nanomanufacturing of silicon surface with a single atomic layer precision via mechanochemical reactions, Nat. Commun. **9**, 1542 (2018).

[18] J. S. Bhamra, J. P. Ewen, C. A. Latorre, J. A. R. Bomidi, M. W. Bird, N. Dasgupta, A. C. T. van Duin, and D. Dini, Interfacial bonding controls friction in diamond-rock contacts, J. Phys. Chem. C **125**, 18395 (2021).

[19] Y. Lu, C. Xiao, Y. Jiang, C. Tang, L. Chen, J. Sun, and L. Qian, Nanoscale wear triggered by stress-driven electron transfer, Nano Lett. **23**, 8842 (2023).

[20] A. Erbaş, D. Horinek, and R. R. Netz, Viscous friction of hydrogen-bonded matter, J. Am. Chem. Soc. **134**, 623 (2012).

[21] J. Chen, I. Ratera, J. Y. Park, and M. Salmeron, Velocity dependence of friction and hydrogen bonding effects, Phys. Rev. Lett. **96**, 236102 (2006).

[22] L. Peng, F. Hsia, S. Woutersen, M. Bonn, B. Weber, and D. Bonn, Nonmonotonic friction due to water capillary adhesion and hydrogen bonding at multiasperity interfaces, Phys. Rev. Lett. **129**, 256101 (2022).

[23] T. Poiesz, S. Achanta, J. Bouwknegt, and AA Soethoudt, Substrate holder and a method of manufacturing a substrate holder, U.S. Patent No. 11,086,234 (2021).

[24] A. I. Vakis, V. A. Yastrebov, J. Scheibert, L. Nicola, D. Dini, C. Minfray *et al.*, Modeling and simulation in tribology across scales: An overview, Tribol. Int. **125**, 169 (2018).

[25] O. Ben-David, S. M. Rubinstein, and J. Fineberg, Slip-stick and the evolution of frictional strength, Nature (London) **463**, 76 (2010).

[26] B. Weber, T. Suhina, A. M. Brouwer, and D. Bonn, Frictional weakening of slip interfaces, Sci. Adv. **5**, 1 (2019).

[27] S. Dillavou and S. M. Rubinstein, Nonmonotonic aging and memory in a frictional interface, Phys. Rev. Lett. **120**, 224101 (2018).

[28] C. H. Scholz, Earthquakes and friction laws, Nature (London) **391**, 37 (1998).

[29] Y. Xing and E. Borguet, Specificity and sensitivity of fluorescence labeling of surface species, Langmuir **23**, 684 (2007).

[30] J. D. Cyran, M. A. Donovan, D. Vollmer, F. S. Brigiano, S. Pezzotti, D. R. Galimberti, M-P. Gaigeot, M. Bonn, and E. H. G. Backus *et al.*, Molecular hydrophobicity at a macroscopically hydrophilic surface, Proc. Natl. Acad. Sci. U.S.A. **116**, 1520 (2019).

[31] L. T. Zhuravlev, The surface chemistry of amorphous silica. Zhuravlev model, Colloids Surf., A **173**, 1 (2000).

[32] K. Tian, N. N. Gosvami, D. L. Goldsby, Y. Liu, I. Szlufarska, and R. W. Carpick, Load and time dependence of interfacial chemical bond-induced friction at the nanoscale, Phys. Rev. Lett. **118**, 076103 (2017).

[33] See Supplemental Material at http://link.aps.org/supplemental/10.1103/PhysRevLett.131.226201 for details about boundary element method calculations, experimental result of friction force as a function of the number of sliding strokes, optical images of the silicon ball recorded before and after the friction measurement, rms and average roughness of the silicon wafer surfaces before and after plasma cleaning, friction force and water contact angle as a function of aging time at 40% relative humidity, and fluorescence spectra and images of the plasma-cleaned wafer surfaces after different nitrogen drying times, which includes Refs. [34–40].

[34] F. Hsia, C. Hsu, L. Peng, F. M. Elam, C. Xiao, S. Franklin *et al.*, Contribution of capillary adhesion to friction at macroscopic solid-solid interfaces, Phys. Rev. Appl. **17**, 034034 (2023).

[35] A. Akchurin, R. Bosman, P. M. Lugt, and M. Van Drogen, On a model for the prediction of the friction coefficient in mixed lubrication based on a load-sharing concept with measured surface roughness, Tribol. Lett. **59**, 1 (2015).

[36] M. H. Müser, W. B. Dapp, R. Bugnicourt, P. Sainsot, N. Lesaffre, T. A. Lubrecht *et al.*, Meeting the contact-mechanics challenge, Tribol. Lett. **65**, 1 (2017).

[37] A. Gujrati, S. R. Khanal, L. Pastewka, and T. D. B. Jacobs, Combining TEM, AFM, and profilometry for quantitative topography characterization across all scales, ACS Appl. Mater. Interfaces **10**, 29169 (2018).

[38] T. D. B. Jacobs, K. E. Ryan, P. L. Keating, D. S. Grierson, J. A. Lefever, K. T. Turner, J. A. Harrison, and R. W. Carpick, The effect of atomic-scale roughness on the adhesion of nanoscale asperities: A combined simulation and experimental investigation, Tribol. Lett. **50**, 81 (2013).

[39] T. D. B. Jacobs and L. Pastewka, Surface topography as a material parameter, MRS Bull. **47**, 1205 (2022).

[40] C. Leriche, C. Xiao, S. Franklin, and B. Weber, From atomic attrition to mild wear at multi-asperity interfaces: The wear of hard Si_3N_4 repeatedly contacted against soft Si, Wear **528–529**, 204975 (2023).

[41] A. U. Alam, M. M. R. Howlader, and M. J. Deen, The effects of oxygen plasma and humidity on surface roughness, water contact angle and hardness of silicon, silicon dioxide and glass, J. Micromech. Microeng. **24**, 035010 (2014).

[42] S. M. Hong, S. H. Kim, J. H. Kim, and H. I. Hwang, Hydrophilic surface modification of PDMS using atmospheric RF plasma, J. Phys. Conf. Ser. **34**, 656 (2006).

[43] P. N. Nge, C. I. Rogers, and A. T. Woolley, Advances in microfluidic materials, functions, integration, and applications, Chem. Rev. **113**, 2550 (2013).

[44] H. Hillborg, N. Tomczak, A. Olàh, H. Schönherr, and G. J. Vancso, Nanoscale hydrophobic recovery: A chemical force microscopy study of UV/ozone-treated cross-linked poly (dimethylsiloxane), Langmuir **20**, 785 (2004).

[45] D. Bodas and C. Khan-Malek, Formation of more stable hydrophilic surfaces of PDMS by plasma and chemical treatments, Microelectron. Eng. **83**, 1277 (2006).

[46] C. S. Ewing, S. Bhavsar, G. Veser, Mc. J. J. Carthy, and J. K. Johnson, Accurate amorphous silica surface models from first-principles thermodynamics of surface dehydroxylation, Langmuir **30**, 5133 (2014).

[47] O. Sneh and S. M. George, Thermal stability of hydroxyl groups on a well-defined silica surface, J. Phys. Chem. **99**, 4639 (1995).

[48] T. S. Williams and R. F. Hicks, Aging mechanism of the native oxide on silicon (100) following atmospheric oxygen plasma cleaning, J. Vac. Sci. Technol. A **29**, 041403 (2011).

[49] K. Tian, Z. Li, N. N. Gosvami, D. L. Goldsby, I. Szlufarska, and R. W. Carpick, Memory distance for interfacial chemical bond-induced friction at the nanoscale, ACS Nano **13**, 7425 (2019).

[50] J. N. Israelachvili and M. L. Gee, Contact angles on chemically heterogeneous surfaces, Langmuir **5**, 288 (1989).

[51] L. Dalstein, E. Potapova, and E. Tyrode, The elusive silica/water interface: Isolated silanols under water as revealed by vibrational sum frequency spectroscopy, Phys. Chem. Chem. Phys. **19**, 10343 (2017).

[52] R. N. Lamb and D. N. Furlong, Controlled wettability of quartz surfaces, J. Chem. Soc. Faraday Trans. 1 Phys. Chem. Condens. Phases **78**, 61 (1982).

[53] A. Rimola, D. Costa, M. Sodupe, J. F. Lambert, and P. Ugliengo, Silica surface features and their role in the adsorption of biomolecules: Computational modeling and experiments, Chem. Rev. **113**, 4216 (2013).

[54] E. A. McArthur, T. Ye, J. P. Cross, S. Petoud, and E. Borguet, Fluorescence detection of surface-bound intermediates produced from UV photoreactivity of alkylsiloxane SAMs, J. Am. Chem. Soc. **126**, 2260 (2004).
[55] F. Zhang, K. Sautter, A. M. Larsen, D. A. Findley, R. C. Davis, H. Samha, and M. R. Linford, Chemical vapor deposition of three aminosilanes on silicon dioxide: Surface characterization, stability, effects of silane concentration, and cyanine dye adsorption, Langmuir **26**, 14648 (2010).
[56] C. Funk, P. M. Dietrich, T. Gross, H. Min, W. E. S. Unger, and W. Weigel, Epoxy-functionalized surfaces for microarray applications: Surface chemical analysis and fluorescence labeling of surface species, Surf. Interface Anal. **44**, 890 (2012).
[57] L. Pastewka and M. O. Robbins, Contact between rough surfaces and a criterion for macroscopic adhesion, Proc. Natl. Acad. Sci. U.S.A. **111**, 3298 (2014).
[58] A. Tiwari, J. Wang, and B. N. J. Persson, Adhesion paradox: Why adhesion is usually not observed for macroscopic solids, Phys. Rev. E **102**, 042803 (2020).
[59] P. Schwaderer, E. Funk, F. Achenbach, J. Weis, C. Bräuchle, and J. Michaelis, Single-molecule measurement of the strength of a siloxane bond, Langmuir **24**, 1343 (2008).
[60] F.-C. Hsia, S. Franklin, P. Audebert, A. M. Brouwer, D. Bonn, and B. Weber, Rougher is more slippery: How adhesive friction decreases with increasing surface roughness due to the suppression of capillary adhesion, Phys. Rev. Res. **3**, 043204 (2021).
[61] T. Plach, K. Hingerl, S. Tollabimazraehno, G. Hesser, V. Dragoi, and M. Wimplinger, Mechanisms for room temperature direct wafer bonding, J. Appl. Phys. **113** (2013).
[62] J. R. Rice and A. L. Ruina, Stability of steady frictional slipping, J. Appl. Mech. Trans. ASME **50**, 343 (1983).
[63] T. Baumberger and C. Caroli, Solid friction from stick-slip down to pinning and aging, Adv. Phys. **55**, 279 (2006).
[64] I. Barel, M. Urbakh, L. Jansen, and A. Schirmeisen, Multibond dynamics of nanoscale friction: The role of temperature, Phys. Rev. Lett. **104**, 066104 (2010).
[65] Z. Li and I. Szlufarska, Multiphysics model of chemical aging in frictional contacts, Phys. Rev. Mater. **2**, 063602 (2018).